Modeling and Iron-Effect Analysis on Magnetic Field and Torque Output of Electromagnetic Spherical Actuators With Iron Stator

Liang Yan, *Member, IEEE*, I-Ming Chen, *Senior Member, IEEE*, Chee Kian Lim, *Member, IEEE*, Guilin Yang, *Member, IEEE*, and Kok-Meng Lee, *Fellow, IEEE*

***Abstract*—This paper presents a three-degree-of-freedom permanent magnet (PM) spherical actuator with an iron stator. The major contribution of this paper is to study the effect of iron stator on the magnetic field and torque output of the electromagnetic spherical actuator quantitatively and qualitatively. It could be helpful for actuator design optimization. Based on the poles' arrangement and the iron boundary, the magnetic field of the PM-pole rotor and the actuator torque are formulated analytically. The effect of iron stator on the magnetic field and torque output is analyzed with respect to structural parameters. The result shows that the iron stator can increase the radial component of the flux density and thus the actuator torque output significantly.**

***Index Terms*—Actuators, magnetic fields, modeling, permanent-magnet motors, torque.**

I. Introduction

A spherical actuator is a device that can generate multi-degree-of-freedom (multi-DOF) rotational motions in a single joint. It has wide potential applications in robotic joints, flexible machining, precision assembling, and omnidirectional wheels, due to its compact structure, low inertia moment and nonsingularity in workspace. Williams and Laithwaite [1] have designed the first 2-DOF spherical induction motor. The rotor is made of ferromagnetic material with a spherical barrel-shaped surface. A copper mesh is inlaid on the rotor surface to allow induction current to travel in longitudinal and latitudinal directions. The laminated stator consists of two multiphase winding blocks that can create a rotational magnetic field, and thus induce the current on the surface of the rotor. The interaction between the induced current and the stator magnetic field produces a 2-DOF motion on the rotor. Davey *et al.* [2] derived the torque model of this induction motor by integrating the Maxwell stress moment over the spherical rotor surface. A 3-DOF induction spherical motor was conceptualized by Vachtsevanos *et al.* [3]. Three sets of windings are mounted on the stator and excited to generate induced current on the rotor surface, and thus to drive the rotor to achieve 3-DOF rotations. The mechanical complexity and the inherent poor servo characteristics of this spherical induction motor led Lee *et al.* [4] to develop a 3-DOF spherical stepper based on the principle of variable-reluctance. Coils are mounted on a hemispheric stator structure with iron teeth, whereas a pair of PM poles are assembled on the nonmagnetic rotor. By energizing the stator coils sequentially, the rotor is pulled to desired positions. Permanent-magnet (PM) spherical actuators that can achieve 2/3-DOF motion are developed by Wang *et al.* [5]. The rotor is housed within the spherical hollow stator on a low friction surface coating. On the application of current to the stator windings, the resulting torque can orientate the rotor to certain positions. Chirikjian *et al.* [6] made a spherical stepper with a PM-pole plastic rotor and a stator with an array of coils. Difference in the symmetric layout of rotor and stator poles allows stepping motion in three orientations. Yang *et al.* [7] proposed a 3-DOF spherical actuator composed of a rotor with two magnet poles and a stator with five electromagnet poles. Through the interaction of rotor and stator magnetic fields, the rotor can make an arbitrary orientation and a spin. Kahlen *et al.* [8] developed a spherical motor consisting of a rotor with 112 PM poles and a stator with 96 windings. The stator hemisphere and the stator poles are made of a soft-magnetic composite. The poles were arranged symmetrically corresponding to longitude and latitude of a globe. Supplied current in the coils interacts with the magnetic field by the stator, and thus produces 3-DOF rotor motions. The actuator torque was calculated numerically. More recently, Dehez *et al.* [9] developed a 2-DOF spherical induction motor composed of a two-layer rotor with teeth surrounded by five inductors on the laminated stator. The inductors generate a slipping magnetic field on the rotor, and thus move it in 2-DOF. The rotor can achieve unlimited angular range. Lee *et al.* [10]–[13] have developed a spherical wheel motor based on the principle of variable reluctance. Eight PM pole pairs are mounted on the rotor, whereas ten electromagnet pole pairs on the ferromagnetic stator. It offers a means to control the orientation of a rotating shaft in an open-loop

Manuscript received July 14, 2010; revised February 7, 2011; accepted April 24, 2011. Date of publication July 7, 2011; date of current version August 24, 2012. This work was supported by the National Nature Science Foundation of China and the Fundamental Research Funds for the Central Universities. Recommended by Technical Editor D. Caldwell.

L. Yan is with the School of Automation Science and Electrical Engineering, Beihang University, Beijing, China 100191 (e-mail: Lyan1991@gmail.com).

I.-M. Chen is with the School of Mechanical and Aerospace Engineering, Nanyang Technological University, Singapore 637098 (e-mail: michen@ntu.edu.sg).

C. K. Lim is with the School of Mechanical and Aeronautical Engineering, Singapore Polytechnic, Singapore 139651 (e-mail: lim_chee_kian@sp.edu.sg).

G. Yang is with the Mechatronics Group, Singapore Institute of Manufacturing Technology, Singapore 638075 (e-mail: glyang@simtech.a-star.edu.sg).

K.-M. Lee is with the George W. Woodruff School of Mechanical Engineering, Georgia Institute of Technology, Atlanta, GA 30332-0405 USA (e-mail: kokmeng.lee@me.gatech.edu).

Color versions of one or more of the figures in this paper are available online at http://ieeexplore.ieee.org.

Digital Object Identifier 10.1109/TMECH.2011.2159238

fashion. Ueno *et al.* [14] proposed a miniature spherical motor using iron gallium alloy (Galfenol) consisting of four rods of Galfenol with square cross-section, a wound coil, a permanent magnet, an iron yoke and a spherical rotor placed on the edge of the rods. When currents of 180 phase difference flow in pairs of opposing coils, a torque is exerted on the rotor by pushing (expansion) and pulling (contraction) of the rods.

In our study, a spherical actuator with layers of PM rotor poles and stator air-core coils has been proposed. One of the major features of this spherical actuator is that the structure of two force/torque generating elements, PM and coil poles, are parameterized, which helps us to observe the relationship between structural parameters and torque output. This provides a way to increase the actuator torque by selecting structure dimensions. In the first stage [15], an aluminum stator is employed for the actuator design. However, it was found that the torque output is not very high. Therefore, the objective of this paper is to propose a design concept of the PM spherical actuator with iron stator to increase the torque output, because high permeability of ferromagnetic material may help to reduce the magnetic energy loss, and thus to increase the force to the power ratio. Although spherical actuators with iron stators have been developed previously [2], [10], [16], there is no detailed analysis on the iron effect. This paper studies the iron effect on magnetic field and torque output quantitatively and qualitatively, which could be useful for design optimization of actuator structural parameters. Unlike conventional motors with soft iron in the magnetic loop, the employment of ferromagnetic material in this actuator design does not affect the linearity of the torque model. A multichannel current controller has been developed to regulate the currents independently in the stator coils, and thus to drive the rotor to any orientation within the workspace.

II. Formulation of the Magnetic Field

Analysis of PM rotor's magnetic field is a precondition of torque modeling that in turn is significant for actuator control. The challenge of magnetic field formulation for spherical actuators is that the flux density is a vector that varies in three-dimensional (3D) space. In this study, Laplace's equation is employed to solve the magnetic scalar potential, and thus to formulate the magnetic field distribution analytically.

A. Assumptions

1) The magnetic permeability of air space is the same as that of free space.
2) The magnetic permeability of stator iron is much greater than that of air space.
3) PMs are assumed to be ideal with field relationship described by the linear second quadrant of a PM demagnetization curve.
4) PM poles are magnetized uniformly.
5) The medium in the magnetic field is homogenous.

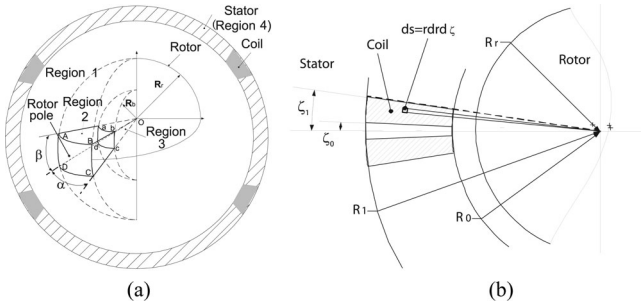

Fig. 1. Geometry of rotor and stator poles. (a) Rotor and stator space. (b) Sectional view of the coil shape.

B. Geometry of Rotor and Stator Poles

Due to the high power density of PM, it is widely used for design of actuators [17]. As illustrated in Fig. 1(a), the proposed spherical actuator consists of a rotor with alternatively magnetized PM poles along the equator, and an iron stator with two layers of air-core coils. Fig. 1(a) presents the shape of a single rotor pole - an approximated dihedral cone enclosed by $ABCD$ and $abcd$ that can be specified by four parameters: α, β, $R_{r,}$ and R_b. Conical-shaped coil [see Fig. 1(b)] is specified by four parameters, i.e., R_0, R_1, ζ_0, and ζ_1. This geometric shape can take advantage of the space surrounding the rotor effectively, and facilitate the actuator torque formulation in the spherical coordinates.

C. Characterization of Rotor Space

The three regions in Fig. 1(a) are characterized by

$$\mathbf{B}_1 = \mu_0 \mathbf{H}_1, \mathbf{B}_2 = \mu_0 \mu_m \mathbf{H}_2 + \mu_0 \mathbf{M}_0, \mathbf{B}_3 = \mu_0 \mu_r \mathbf{H}_3 \quad (1)$$

where $\mathbf{B}$ is flux density and $\mathbf{H}$ is magnetic intensity. The subscripts "$1, 2, 3$" denote Region 1 (air space surrounding the rotor), 2 (PM rotor poles), and 3 (ferromagnetic rotor core) respectively. μ_0, μ_m, and μ_r are magnetic permeability of free space (H/m), relative recoil permeability of PM and relative permeability of ferromagnetic materials respectively. $\mathbf{M}_0 = \mathbf{B}_{\text{rem}}/\mu_0$ is the residual magnetization vector in A/m. In spherical coordinates, the residual magnetization vector of the pth PM is expressed as

$$\mathbf{M}_0 = \begin{bmatrix} M_{0,r} \\ M_{0,\theta} \\ M_{0,\phi} \end{bmatrix} = (-1)^{p-1} |\mathbf{M}_0| \begin{bmatrix} \cos(\phi - \alpha_p) \sin\theta \\ \cos(\phi - \alpha_p) \cos\theta \\ -\sin(\phi - \alpha_p) \end{bmatrix} \quad (2)$$

where $\alpha_p = \alpha/2 + 2\pi(p-1)/P, p = 1, 2, \ldots, P$. P is the total number of PM poles. And (2) is only valid in

$$0 < \phi - \frac{2\pi(p-1)}{P} < \alpha, \frac{\pi}{2} - \frac{\beta}{2} < \theta < \frac{\pi}{2} + \frac{\beta}{2}.$$

D. Laplace's Equations and Solution

$\mathbf{H}$ is curl free and can thus be expressed in terms of a scalar potential function Φ in spherical coordinates

$$\mathbf{H} = -\nabla\Phi = H_r \mathbf{e}_r + H_\theta \mathbf{e}_\theta + H_\phi \mathbf{e}_\phi \quad (3)$$

where $\mathbf{e}_r$, $\mathbf{e}_\theta$, and $\mathbf{e}_\phi$ are respective unit vectors, H_r, H_θ, and H_ϕ are components of magnetic field intensity $\mathbf{H}$. The scalar potentials are governed by the Laplace's equations

$$\nabla^2 \Phi_i = 0 \tag{4}$$

where $i = 1, 2, 3$. The general solution of Φ_i is

$$\Phi_i = \sum_{n=0}^{\infty} \sum_{m=-n}^{n} (\kappa_{n,i}^m r^n + \xi_{n,i}^m r^{-(n+1)}) Y_n^m(\theta, \phi) \tag{5}$$

where $\kappa_{n,i}^m$ and $\xi_{n,i}^m$ are coefficients. The angular part of the solutions to the Laplace's equation, Y_n^m, is a complex valued spherical harmonic function defined by

$$Y_n^m(\theta, \phi) = S_n^m P_n^m(\cos\theta) e^{im\phi},$$

where $S_n^m = \sqrt{\dfrac{2n+1}{4\pi} \dfrac{(n-m)!}{(n+m)!}}$; n, m are integers with the condition $-n \le m \le n$.

E. Boundary Conditions

The particular solutions that characterize the magnetic scalar potentials of three regions require the specification of the source term and the six unknowns, $\kappa_{n,i}^m$ and $\xi_{n,i}^m$. The unknowns can be solved from boundary conditions (BC):

1) $B_{1,\theta}|_{r=Rs} = 0$, $B_{1,\phi}|_{r=Rs} = 0$,
2) $B_{1,r}|_{r=R_r} = B_{2,r}|_{r=R_r}$, $B_{2,r}|_{r=R_b} = B_{3,r}|_{r=R_b}$,
3) $H_{1,\phi}|_{r=R_r} = H_{2,\phi}|_{r=R_r}$, $H_{1,\theta}|_{r=R_r} = H_{2,\theta}|_{r=R_r}$,
4) $B_{3,r}|_{r=0}$, $B_{3,\theta}|_{r=0}$, $B_{3,\phi}|_{r=0} \neq \infty$,
5) $H_{2,\phi}|_{r=R_b} = H_{3,\phi}|_{r=R_b}$, $H_{2,\theta}|_{r=R_b} = H_{3,\theta}|_{r=R_b}$,

where R_b, R_r, and R_s are rotor core radius, rotor radius, and the stator radius, respectively.

F. Solution of Magnetic Flux Density

1) Solution of Unknowns in Scalar Potential: According to Lorentz force law, only the magnetic field in Region 1 (air) generates actuator torque. Therefore, solutions of $\xi_{n,1}^m$ and $\kappa_{n,1}^m$ are important for solving magnetic field distribution. By using BC, the following results can be achieved

$$\kappa_{n,1}^m = O_{n,5} C_{nm}, \quad \xi_{n,1}^m = O_{n,6} C_{nm} \tag{6}$$

where

$$\begin{aligned}
O_{n,6} &= -(O_{n,3}/O_{n,4} R_r^{2n+1} - O_{n,2}/O_{n,1})/(R_r^{2n+1} - R_s^{2n+1}) \\
&\quad \times R_s^{2n+1} \\
O_{n,5} &= (O_{n,3}/O_{n,4} R_r^{2n+1} - O_{n,2}/O_{n,1})/(R_r^{2n+1} - R_s^{2n+1}) \\
O_{n,4} &= [(\mu_r - \mu_m) n R_b^{2n+1}] \\
O_{n,3} &= [\mu_r n + \mu_m (n+1)] O_{n,2}/O_{n,1} - R_b^{n+2} \\
O_{n,2} &= R_r^{n+2} (R_r^{2n+1} - R_s^{2n+1})(\mu_r - \mu_m) n R_b^{2n+1} \\
&\quad - R_b^{n+2} R_r^{2n+1} \\
&\quad \{n R_r^{2n+1} (1 - \mu_m) + (n + 1 + \mu_m n) R_s^{2n+1}\} \\
O_{n,1} &= \{[n + \mu_m (n+1)] R_r^{2n+1} \\
&\quad + [(n+1) - \mu_m (n+1)] R_s^{2n+1}\} \\
&\quad (\mu_r - \mu_m) n R_b^{2n+1} - R_r^{2n+1} \{n R_r^{2n+1} (1 - \mu_m) \\
&\quad + (n + 1 + \mu_m n) R_s^{2n+1}\} [\mu_r n + \mu_m (n+1)].
\end{aligned}$$

2) Scalar Potential and Flux Density: Using $\kappa_{n,1}^m$ and $\xi_{n,1}^m$ and discarding high-order harmonic terms give

$$\begin{aligned}
\Phi_1 &= \frac{3}{8} \sqrt{\frac{35}{2\pi}} \frac{cM_0}{\sqrt{\pi}} [O_{4,5} r^4 + O_{4,6} r^{-5}] \\
&\quad \times \sin^4\theta (a \cos 4\phi - b \sin 4\phi).
\end{aligned} \tag{7}$$

a and c in (7) are calculated with

$$a \pm bi \equiv \int_0^{2\pi} f(\phi) e^{-im\phi} d\phi (m = 4 \text{ and } m = -4), \tag{8}$$

$$c/\sqrt{\pi} \equiv \int_0^{\pi} S_n^m \sin^2\theta [P_n^m(\cos\theta)] d\theta,$$

$$f(\phi) = (-1)^{p-1} \cos\left[\phi - \frac{\pi}{4}(p-1)\right], p = 1, 2, \ldots, 8. \tag{9}$$

Therefore, three components of the magnetic flux density are calculated as (To simplify the equation, let $\alpha_0 = 0$.)

$$\begin{aligned}
B_{1,r} &= \frac{3}{8} \sqrt{\frac{35}{2\pi}} \frac{ac\mu_0 M_0}{\sqrt{\pi}} [5 O_{4,6} r^{-6} - 4 O_{4,5} r^3] \\
&\quad \times \sin^4\theta \cos 4\phi
\end{aligned} \tag{10}$$

$$\begin{aligned}
B_{1,\theta} &= -\frac{3}{2} \sqrt{\frac{35}{2\pi}} \frac{ac\mu_0 M_0}{\sqrt{\pi}} [O_{4,5} r^3 + O_{4,6} r^{-6}] \\
&\quad \times \sin^3\theta \cos\theta \cos 4\phi
\end{aligned} \tag{11}$$

$$B_{1,\phi} = \frac{3}{2} \sqrt{\frac{35}{2\pi}} \frac{ac\mu_0 M_0}{\sqrt{\pi}} [O_{4,5} r^3 + O_{4,6} r^{-6}] \sin^3\theta \sin 4\phi. \tag{12}$$

III. Torque Modeling

A. Torque Generated by a Single Coil

The current passing through the section area of $d\mathbf{l}$ in Fig. 1(b) is $Jrdrd\zeta$, where J is the current density in the section area of coil. Therefore, the torque on a single coil is

$$\mathbf{T}_c = -J \int_{R_0}^{R_1} \int_{\zeta_0}^{\zeta_1} \left\{ \int_C r B_{1,r}(r, \theta, \phi) d\mathbf{l} \right\} r dr d\zeta. \tag{13}$$

With $B_{1,r}$ and (13), the actuator torque generated by the ith coil, denoted as $\mathbf{T}_i$, can be expressed explicitly using the ith coil-axis position θ_i and ϕ_i with respect to the rotor frame, as well as the current input J_i passing through this coil, i.e.,

$$\mathbf{T}_i = [T_{ix}, T_{iy}, T_{iz}]^{\mathrm{T}} = T_c \mathbf{G}(\theta_i, \phi_i) J_i \tag{14}$$

where

$$\begin{aligned}
\mathbf{G}(\theta_i, \phi_i) &= [g_x(\theta_i, \phi_i), g_y(\theta_i, \phi_i), g_z(\theta_i, \phi_i)]^{\mathrm{T}} \\
&= \mathbf{e}_{\phi i} (-4 \sin^3\theta_i \cos^4\phi_i \cos\theta_i \\
&\quad - 4 \sin^3\theta_i \sin^4\phi_i \cos\theta_i \\
&\quad + 24 \sin^3\theta_i \cos^2\phi_i \sin^2\phi_i \cos\theta_i) - \mathbf{e}_{\theta i} (16 \sin^3\theta_i
\end{aligned}$$

$$\times \cos^3\phi_i \sin\phi_i - 16\sin^3\theta_i \sin^3\phi_i \cos\phi_i)$$

$$T_c = \frac{15}{8}\sqrt{\frac{35}{2}}\mu_0 M_0 acR_c G_\zeta$$

$$R_c = O_{4,6}R_{c,1} + O_{4,5}R_{c,2}$$

$$R_{c,1} = (R_0^{-2} - R_1^{-2})/2, R_{c,2} = (R_0^7 - R_1^7)/7$$

$$G_\zeta = G''_\zeta - \frac{3G'_\zeta}{4}, G'_\zeta = 1/5\sin^5\zeta_1 - 1/5\sin^5\zeta_0$$

$$G''_\zeta = 1/5\cos^4\zeta_0\sin\zeta_0 - 1/15\cos^2\zeta_0\sin\zeta_0 - 2/15\sin\zeta_0 - 1/5\cos^4\zeta_1\sin\zeta_1 + 1/15\cos^2\zeta_1\sin\zeta_1 + 2/15\sin\zeta_1$$

$$\mathbf{e}_{\phi i} = -\sin\phi_i\mathbf{e}_x + \cos\phi_i\mathbf{e}_y$$

$$\mathbf{e}_{\theta i} = \cos\theta_i\cos\phi_i\mathbf{e}_x + \cos\theta_i\sin\phi_i\mathbf{e}_y - \sin\theta_i\mathbf{e}_z. \quad (15)$$

B. Torque Model for Actuator with Full Set of Coils

With N coils on the stator, torque model of the spherical actuator with a complete set of coils is obtained

$$\mathbf{T} = T_c Q\mathbf{J} \quad (16)$$

where $\mathbf{J} = [\,J_1 \quad J_2 \quad \ldots \quad J_N\,]^{\mathrm{T}}$ is current passing through N coils, and Q is torque matrix

$$Q = \begin{bmatrix} f_x(\theta_1,\phi_1) & f_x(\theta_2,\phi_2) & \ldots & f_x(\theta_N,\phi_N) \\ f_y(\theta_1,\phi_1) & f_y(\theta_2,\phi_2) & \ldots & f_y(\theta_N,\phi_N) \\ f_z(\theta_1,\phi_1) & f_z(\theta_2,\phi_2) & \ldots & f_z(\theta_N,\phi_N) \end{bmatrix}.$$

Unlike single-axis motor [18], the torque output of spherical actuator is dependent on the rotor orientation and current input. Generally, motors with soft iron in the magnetic loop have nonlinear torque models. However, from (14), the torque model of this spherical actuator is in a linear fashion, which can greatly facilitate the real-time motion control of the actuator. This torque model may be applied to spherical actuators with either ferromagnetic or nonferromagnetic stator.

IV. Effect Analysis of an Iron Stator

In this section, the derived theoretical models are used to analyze the effect of iron stator on the magnetic field distribution and torque output of the actuator.

A. Effect Analysis of Iron Stator on the Magnetic Field

Denoting components $5O_{4,6}r^{-6} - 4O_{4,5}r^3$, $O_{4,5}r^3 + O_{4,6}r^{-6}$, and $O_{4,5}r^3 + O_{4,6}r^{-6}$ in (10)–(12), as $O_{s,1}$, $O_{s,2}$, and $O_{s,3}$ respectively gives

$$B_{1,r} = \frac{3}{8}\sqrt{\frac{35}{2\pi}}\frac{ac\mu_0 M_0}{\sqrt{\pi}}O_{s,1}\sin^4\theta\cos 4\phi, \quad (17)$$

$$B_{1,\theta} = -\frac{3}{2}\sqrt{\frac{35}{2\pi}}\frac{ac\mu_0 M_0}{\sqrt{\pi}}O_{s,2}\sin^3\theta\cos\theta\cos 4\phi, \quad (18)$$

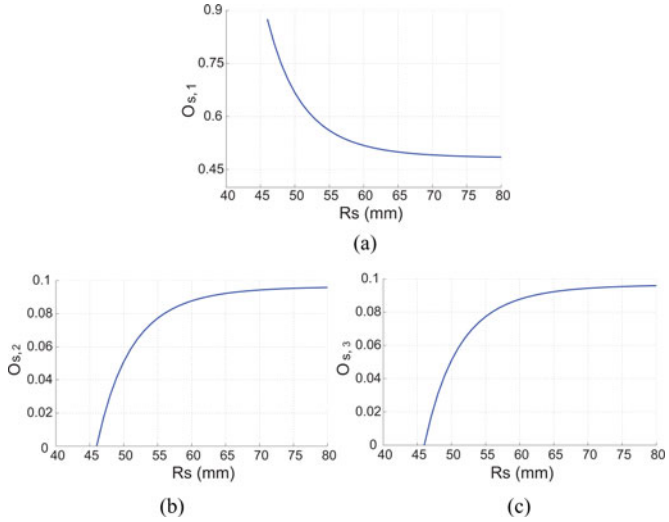

Fig. 2. Relationship between flux density and stator radius ($r = 46.5$ mm). (a) $O_{s,1}$ versus R_s. (b) $O_{s,2}$ versus R_s. (c) $O_{s,3}$ versus R_s.

$$B_{1,\phi} = \frac{3}{2}\sqrt{\frac{35}{2\pi}}\frac{ac\mu_0 M_0}{\sqrt{\pi}}O_{s,3}\sin^3\theta\sin 4\phi. \quad (19)$$

The relationship between magnetic flux density components and stator radius can be revealed through the relationships between $O_{s,1}, O_{s,2}, O_{s,3}$ and stator radius R_s as presented in Fig. 2. The figure indicates following results.

1) $O_{s,2}$ and $O_{s,3}$ are equal to zero when stator radius is approximately the same as the rotor radius. In other words, the tangential components of flux density $B_{1,\theta}$ and $B_{1,\phi}$ are nearly equal to zero when the stator radius approaches the rotor radius.
2) $O_{s,1}$ is larger with the smaller size of stator radius, which indicates that most fluxes in ϕ- and θ-directions are "dragged" to the r-direction due to high permeability of the stator iron. As a result, the flux leakage starts small when the stator radius decreases.
3) The largest value of $O_{s,1}$ (when $R_s = 46.5$ mm) is about twice the smallest one (when R_s is very large). When the stator size is very large, it can be regarded that the stator is made of nonferromagnetic material. Therefore, the magnetic flux density in the r-direction can be increased about twice maximally by using an iron stator.
4) Because the torque output of the spherical actuator is produced by the radial component of magnetic flux density, a stator made of soft iron may help to increase the actuator torque output.

B. Effect Analysis of the Iron Stator on Torque Output

1) Coil with Fixed Size: As the iron stator affects the magnetic field distribution of PM rotor, it may also change the actuator torque output. Let radii of the coil be fixed at $R_0 = 46.5$ mm and $R_1 = 50$ mm, whereas the stator size increases from 50 mm, i.e., the coil is completely housed inside the stator. From (14), it is known that $R_c = O_{4,6}R_{c,1} + O_{4,5}R_{c,2}$, where R_c is directly proportional to the torque constant, and

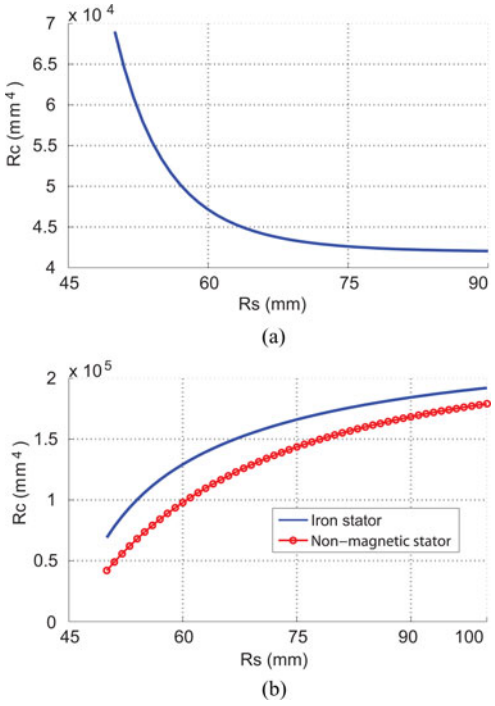

Fig. 3. Relationship between the torque output and stator radius (R_c versus R_s). (a) Fixed coil size. (b) Variable coil size.

$O_{4,5}$, $O_{4,6}$ can be calculated from stator radius, R_s. The computed relationship between R_c and R_s is presented in Fig. 3(a). It can be observed that the value of R_c is large for the small size of the stator. Thus, the actuator torque is also large for small value of R_s. This result is consistent with the effect analysis of the iron stator on the magnetic field distribution. In contrast, in terms of the effect on torque output, an iron stator with infinite size is equivalent to a stator made from nonferromagnetic materials that does not help to increase the torque output. When the stator is made from nonferromagnetic materials, R_c is equal to the lowest value in Fig. 3(a) (4.2×10^4 mm^4). Compared with the nonferromagnetic stator, the iron stator can increase the actuator torque up to 60%.

2) Coil with the Variable Size: The second study of iron stator effect on torque output is based on variable-sized coil, i.e., the external radius of coil, R_1, is equal to the stator radius R_s. Therefore, R_1 will follow the change of R_s. The relationship between R_c and R_s is plotted in Fig. 3(b). The relationship between R_1 and R_s for an aluminum stator is calculated and presented with a dotted line. It can be seen that the solid line is always higher than the dotted line, which indicates that R_c for the iron stator is always larger than that of nonferromagnetic stator with the same size, i.e, the iron stator does help to increase the actuator torque, compared with the nonferromagnetic stator. Furthermore, when the stator size is small, its effect on the torque output is more evident. For example, when the stator outer diameter is about 48 mm, the torque output is nearly doubled with an iron stator, whereas the percentage for torque increase is low for stator with the large size due to the large magnetic flux leakage.

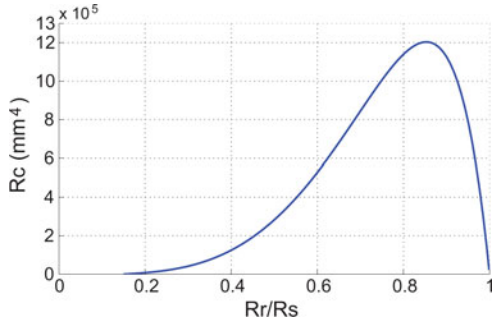

Fig. 4. Relationship between R_c vs. R_r/R_s.

C. Selection of the Rotor and Stator Radii Ratio R_r/R_s

The previous study is based on a rotor with fixed radius. However, in the actuator design, people prefer to fix the stator size, and then find the relationship between torque constant and the ratio of rotor/stator radii. From this relationship, an optimum ratio can be selected, and thus the rotor size is obtained. This approach has advantages as follows.

1) The optimization design of actuator can be considered based on the performance of the whole system including stator and rotor, instead of individual components.
2) The stator radius can be determined in the first place, to satisfy the requirements of the maximum actuator size in various working environment.
3) The use of ratio between rotor and stator radii is regarded as a nondimensional method, so that the actuator torque performance can be analyzed without considering the specific dimensions.

The relationship between R_c in torque constant and R_r/R_s is illustrated in Fig. 4. The maximum value of R_c happens at $R_r/R_s = 0.85$. When R_r/R_s is very low, the rotor size is small, and thus the flux density generated by the rotor is low. As a result, the value of R_c or the torque output is small. When R_r/R_s augments, R_c increases. However, when R_r/R_s is larger than a certain degree, the coil winding is very short. Therefore, R_c and torque output of the actuator decreases correspondingly.

V. Experiment Verification

A. Research Prototype

When the air gap between stator and rotor approaches infinite, it is equivalent to using a stator made from nonferromagnetic materials. Therefore, by letting $R_s = \infty$, the derived magnetic field and torque output models can be applied to spherical actuators with nonferromagnetic stators. Because at current stage we have some problems to fabricate an iron stator, an aluminum stator was utilized to conduct experiment on magnetic field and torque output, and the measurement result is employed to verify analytical models. The developed research prototype is shown in Fig. 5(a). Because of the fixed direction of torque output in single-axis actuators, controllers that have one channel output are utilized to supply power to the actuators. Multiphase output controllers [19], [20] are employed by researchers for

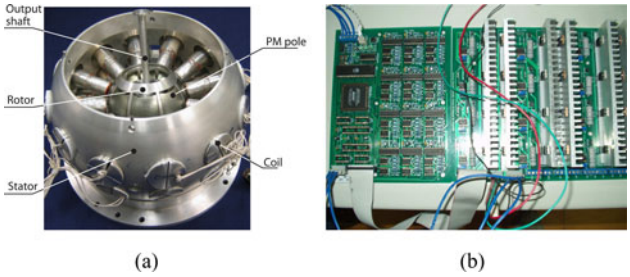

Fig. 5. Research prototype and current controller of spherical actuator. (a) Research prototype. (b) Current controller.

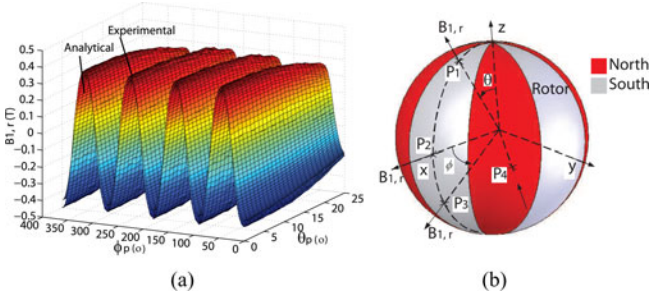

Fig. 6. Comparison of experimental result and analytical model ($B_{1,r}$). (a) Experiment versus analytical result ($d_a = 4.5$ mm). (b) Variation of $B_{1,r}$ on the rotor surface.

electromagnetic machines. However, as the phases are dependant on each other, outputs from these controllers are considered as a single output in nature. Unlike the single-axis actuators, the torque output of spherical actuators includes three orthogonal components that can vary independently. Thus, conventional current controllers cannot be used any more. A multioutput current controller as shown in Fig. 5(b) is utilized in this spherical actuator. Two pieces of this controller will be combined with a 3-DOF rotational sensor that is being developed to regulate the current inputs of coils individually, and thus to achieve high precision real-time close loop motion control of the actuator. The details of the current controller will be introduced in another paper.

B. Experiment on Magnetic Field

1) Magnetic Flux Density $B_{1,r}$ versus θ_p and ϕ_p: Comparisons between experimental result and analytical model are presented in Fig. 6. Fig. 6(a) shows the distribution of $B_{1,r}$ along the longitudinal (ϕ_p) and latitudinal (θ_p) directions ($\theta_p = 0 \sim 25°$, $\phi_p = 0 \sim 360°$) at a fixed radial distance d_a. The analytical and experimental results of the flux density $B_{1,r}$ are approximately the same. In ϕ-direction, there are eight positive/negative peaks, which is consistent with eight alternately magnetized PM poles along the rotor equator. From Fig. 6(b), $B_{1,r}$ is normal to the rotor surface, and reaches the maximum value at the center point of PM pole, P_2. At points far away from the rotor equator such as P_1 and P_3, the flux density becomes smaller due to decreased magnetization volume, with same positive/negative signs. The flux density at the center of the neighboring PM pole, P_4, also has the maximum value, but

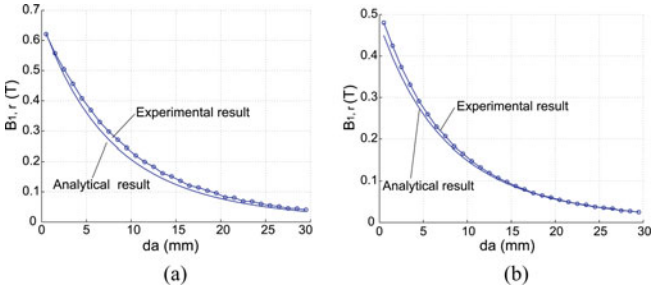

Fig. 7. Variation of magnetic flux density $B_{1,r}$ in radial direction. (a) $\theta_p = 0°$, $\phi_p = 45°$. (b) $\theta_p = 10°$, $\phi_p = 35°$.

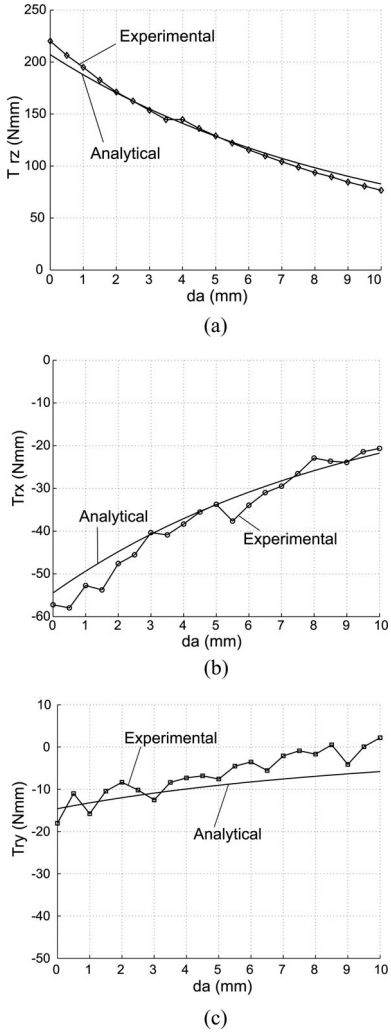

Fig. 8. Torque variation in the radial direction d_a ($\theta_p = 15°$, $\phi_p = 25°$). (a) Torque z (T_{rz}). (b) Torque x (T_{rx}). (c) Torque y (T_{ry}).

with opposite sign. This analysis is coincident with the result in Fig. 6. The difference between experimental data and analytical model is mainly caused by the omission of high-order harmonic terms in developing magnetic scalar potential, the fabrication error of magnets and the measurement error.

2) Magnetic Flux Density $B_{1,r}$ versus d_a: By fixing angular parameters θ_p and ϕ_p ($\theta_p = \pi/2 - \theta, \phi_p = \phi$), the relationship between magnetic flux density $B_{1,r}$ and the air gap between

the measuring point and the rotor surface d_a can be illustrated. Fig. 7 presents the variation of $B_{1,r}$ along the radial direction at ($\theta_p = 0°$, $\phi_p = 45°$) and ($\theta_p = 10°$, $\phi_p = 35°$). It can be seen that the analytical model also fits the experimental result well along the radial direction.

C. Experiment on Torque Output

The torque output of spherical actuator is a 3D vector with components T_x, T_y, and T_z defined in rotor frame. The torque output is a function of the gap between coils and rotor surface. According to the torque model, the actuator torque is related to the coil parameters R_0 and R_1, which in turn can be expressed by the gap d_a between the rotor surface and the coil tip as

$$R_0 = R_r + d_a, R_1 = R_0 + L_c = R_r + d_a + L_c \qquad (20)$$

where L_c is the coil length. By fixing the values of θ_p and ϕ_p, and varying d_a, the relation between torque output and d_a can be obtained. In the torque measurement apparatus, the airgap d_a can be adjusted by screwing the coil in or out the fixture. Fig. 8 shows the torque variation with respect to d_a at (θ_p, ϕ_p) $= (15°, 25°)$. It can be seen that the torque output decreases with the increase of d_a. Therefore, small value of d_a is preferred to achieve high torque output.

VI. Conclusion

The design concept of 3-DOF PM spherical actuators with iron stator is proposed in this paper. Due to the employment of iron stator and air-core coils, the torque output of the spherical actuator increases. Based on the parameters of rotor and stator poles, the magnetic field modeling method with Laplace's equation and the torque modeling method with Lorentz force law are generalized to derive mathematical models for spherical actuators with either ferromagnetic or nonferromagnetic stators. By using the analytical models, the effect of iron stator on the magnetic field distribution and actuator torque output is analyzed qualitatively and quantitatively in various situations. It is found that the use of iron stator can reduce the tangential components and enhance the radial one of the magnetic flux density, and thus increase the torque output of the spherical actuator. As the aluminum stator can be regarded as a special case of the iron stator, experiments are conducted on the existing actuator prototype with aluminum stator to validate the generic models of magnetic field and torque output. The study could facilitate the design optimization of spherical actuators.

References

[1] F. Williams, E. Laithwaite, and J. F. Eastham, "Development and design of spherical induction motors," *Proc. Inst. Elect. Eng.*, vol. 106, pp. 471–484, Dec. 1959.

[2] K. Davey, G. Vachtsevanos, and R. Powers, "The analysis of fields and torques in spherical induction motors," *IEEE Trans. Magn.*, vol. 23, no. 1, pp. 273–282, Jan. 1987.

[3] G. J. Vachtevanos, K. Daveyand, and K. M. Lee, "Development of a novel intelligent robotic manipulator," *IEEE Control Syst. Mag.*, vol. 7, no. 3, pp. 9–15, Jun. 1987.

[4] K. M. Lee and C. K. Kwan, "Design concept development of a spherical stepper for robotic applications," *IEEE Trans. Robot. Autom.*, vol. 7, no. 1, pp. 175–181, Feb. 1991.

[5] J. Wang, G. W. Jewell, and D. Howe, "A novel spherical actuator with three degrees-of-freedom," *IEEE Trans. Magn.*, vol. 34, pp. 2078–2080, Jun. 1998.

[6] G. S. Chirikjian and D. Stein, "Kinematic design and commutation of a spherical stepper motor," *IEEE/ASME Trans. Mechatronics*, vol. 4, no. 4, pp. 342–353, Dec. 1999.

[7] C. Yang and Y. S. Baek, "Design and control of the 3 degrees of freedom actuator by controlling the electromagnetic force," *IEEE Trans. Magn.*, vol. 35, no. 5, pp. 3607–3609, Sep. 1999.

[8] K. Kahlen, I. Voss, C. Priebe, and R. W. De Doncker, "Torque control of a spherical machine with variable pole pitch," *IEEE Trans. Power Electron.*, vol. 19, no. 6, pp. 1628–1634, Nov. 2004.

[9] B. Dehez, G. Galary, and B. Raucent, "Development of a spherical induction motor with two degrees of freedom," *IEEE Trans. Magn.*, vol. 42, no. 8, pp. 2077–2088, Aug. 2006.

[10] K. M. Lee, H. Son, and J. Joni, "Concept development and design of a spherical wheel motor (SWM)," in *Proc. IEEE/ASME Int. Conf. Robot. Autom.*, Jul. 2005, pp. 335–340.

[11] K. M. Lee and H. Son, "Torque model for design and control of a spherical wheel motor," in *Proc. IEEE/ASME Int. Conf. Adv. Intell. Mechatronics*, Jul., 2005, pp. 335–340.

[12] H. Son and K.-M. Lee, "Distributed multipole models for design and control of PM actuators and sensors," *IEEE/ASME Trans. Mechatronics*, vol. 13, no. 2, pp. 228–238, Apr. 2008.

[13] K.-M. Lee, K. Bai, and J. Lim, "Dipole models for forward/inverse torque computation of a spherical motor," *IEEE/ASME Trans. Mechatronics*, vol. 14, no. 1, pp. 46–54, Feb. 2009.

[14] T. Ueno, C. Saito, N. Imaizumi, and T. Higuchi, "Miniature spherical motor using iron–gallium alloy (galfenol)," *Sens. Actuat. A, Phys.*, vol. 154, no. 1, pp. 92–96, Aug. 2009.

[15] L. Yan, I. M. Chen, C. K. Lim, G. Yang, W. Lin, and K. M. Lee, "Design and analysis of a permanent magnet spherical actuator," *IEEE/ASME Trans. Mechatronics*, vol. 13, no. 2, pp. 239–248, Apr. 2008.

[16] K. M. Lee, R. B. Roth, and Z. Zhou, "Dynamic modeling and control of a ball-joint-like variable-reluctance spherical motor," *ASME J. Dyn. Syst., Meas., Control*, vol. 118, pp. 29–40, Mar. 1996.

[17] C. Jo, J.-Y. Seol, and I.-J. Ha, "Flux-weakening control of IPM motors with significant effect of magnetic saturation and stator resistance," *IEEE Trans. Ind. Electron.*, vol. 55, no. 3, pp. 1330–1340, Mar. 2008.

[18] N. Bianchi, S. Bolognani, and M. D. Pre, "Impact of stator winding of a five-phase permanent-magnet motor on postfault operations," *IEEE Trans. Ind. Electron.*, vol. 55, no. 5, pp. 1978–1987, May 2008.

[19] R. Kianinezhad, B. Nahid-Mobarakeh, L. Baghli, F. Betin, and G.-A. Capolino, "Modeling and control of six-phase symmetrical induction machine under fault condition due to open phases," *IEEE Trans. Ind. Electron.*, vol. 55, no. 5, pp. 1966–1977, May 2008.

[20] S. Bachir, S. Tnani, J.-C. Trigeassou, and G. Champenois, "Diagnosis by parameter estimation of stator and rotor faults occurring in induction machines," *IEEE Trans. Ind. Electron.*, vol. 53, no. 3, pp. 963–973, Jun. 2006.

Liang Yan (M'07) received the B.S. degree from North China Institute of Technology, Beijing, China, in 1995, the M.S. degree from Beijing Institute of Technology, Beijing, in 1998, and the Ph.D. degree from Nanyang Technological University, Singapore, in 2006.

From 1998 to 2002, he was a Lecturer at Beijing Institute of Technology. He is currently with Beihang University, Beijing, China. His research interests include actuators, sensors, and navigation system.

Dr. Yan was the recipient of the National Defense Science and Technology Award of China in 2003, and was the Publication Chairman of the 2009 IEEE/ASME International Conference on Advanced Intelligent Mechatronics and 2008 IEEE International Conference on Robotics, Automation, and Mechatronics.

I-Ming Chen (M'95–SM'06) received the B.S. degree from National Taiwan University, Taiwan, China, in 1986, and the M.S. and Ph.D. degrees from California Institute of Technology, Pasadena, in 1989 and 1994, respectively.

He has been with the School of Mechanical and Aerospace Engineering of Nanyang Technological University, Singapore, since 1995. He was with a Japan Society for the Promotion of Science Visiting Scholar at Kyoto University, Kyoto, Japan, in 1999, a Visiting Scholar in the Department of Mechanical Engineering at Massachusetts Institute of Technology, Cambridge, in 2004, and is currently a Fellow of the Singapore-MIT Alliance under the Manufacturing Systems and Technology Program. He is also an Adjunct Professor at Xian Jiao Tong University, Shaanxi, China. His research interests include reconfigurable automation, biomedical applications of reconfigurable robotic systems, parallel kinematics machines, and smart-material-based actuators.

Chee Kian Lim (M'09) received the B.Eng, M.Eng., and Ph.D. degrees from Nanyang Technological University, Singapore, in 1998, 2001 and 2008, respectively.

He is currently a Lecturer in the School of Mechanical and Aeronautical Engineering at Singapore Polytechnic, Singapore. His recent research involves the design of wearable sensors for motion capture and microactuators for wireless capsule endoscopy. His research interests include novel mechatronics systems and design with special focus on electromagnetic and piezoelectric sensors and actuators.

Guilin Yang (M'02) received the B.Eng. and M.Eng. degrees from Jilin University of Technology (now Jilin University), Jilin, China, in 1985 and 1988, respectively, and the Ph.D. degree from Nanyang Technological University, Singapore, in 1999.

Since 1988, he had been with the School of Mechanical Engineering, Shijiazhuang Railway Institute, Hebei, China, as a Lecturer, a Division Head, and then the Vice Dean of the school, for nearly seven years. Currently, he is a Senior Research Scientist and the Group Manager of the Mechanics Group, Singapore Institute of Manufacturing Technology, Singapore. His current research interests include computational kinematics, multibody dynamics, parallel-kinematics machines, modular robots, flexure-based precision mechanisms, electromagnetic actuators, rehabilitation devices, and industrial robot systems. He is currently a technical committee member of the Robotics of the International Federation for the Promotion of Mechanism and Machine Science and the Secretary of the Singapore Chapter of the IEEE Robotics and Automation Society.

Kok-Meng Lee (M'89–SM'02–F'05) received the B.S. degree from the State University of New York, Buffalo, in 1980, and the S.M. and Ph.D. degrees from Massachusetts Institute of Technology, Cambridge, in 1982 and 1985, respectively.

Currently, he is a Professor in the Woodruff School of Mechanical Engineering, Georgia Institute of Technology, Atlanta. His research interests include system dynamics/control, robotics, automation, and mechatronics.

He holds eight patents in machine vision a three degrees of freedom spherical motor/encoder, and a live-bird handling system. Dr. Lee received the National Science Foundation Presidential Young Investigator, Sigma Xi Junior Faculty Research, International Hall of Fame New Technology, and Kayamori Best Paper awards.